

Microstructure, surface morphology and anticancer activity of magnesium doped zinc oxide nanoparticles

P. Pachamuthu^a, A. P. Jeyakumari^{b,*}, N. Srinivasan^c

^a*Department of Physics, Selvam Arts and Science College (Autonomous), Namakkal, Tamilnadu – 637 003, India*

^b*PG and Research Department of Physics, Thiruvalluvar Government Arts College, Rasipuram, Tamilnadu – 637 401, India*

^c*Department of Physics, Kongu Engineering College, Perundurai, Tamilnadu – 638 060, India*

Depending upon their origin and synthesis methods, nanoparticles possess unique physicochemical, structural and morphological characteristics, which are important in a wide variety of applications concomitant to various fields. In the present work, Magnesium doped zinc oxide nanoparticles with different concentrations (5 atomic % and 10 atomic %) are prepared and the prepared samples are annealed at 200 °C for 2 h in a muffle furnace. The structure, surface morphology, chemical composition, optical properties and photoluminescence properties were analyzed using standard procedures. The antioxidant potential and cytotoxicity against the breast cancer MDAMB231 cancer cell line of prepared nanoparticles were explored. A simple, economical soft chemical method was used. The XRD analysis confirmed the presence of hexagonal wurtzite phase with a space group P63mc all the prepared samples. The estimated average grain size for the sample MZ2 (18.16 nm) was smaller than the other samples. The SEM micrograph showed that the morphology of the samples were exhibited the rod shape (MZ1, MZ2 and MZ4) and flower shape (MZ3). The purity of the samples was confirmed by EDAX data. The estimated band gap energy of sample MZ1 and sample MZ3 were 3.41 eV and 3.38 eV from the UV-vis analysis. The FT-IR spectra of the samples predicted the presence of functional groups for Zn-O and Mg-O bonds. The PL analysis displayed a strong UV emission peak at 387 nm and a green emission peak at 557 nm. The results of the prepared samples prove the potential toxicity against MDAMB231 breast cancer cell line.

(Received May 24, 2022; Accepted September 1, 2022)

Keywords: Mg – doped ZnO, XRD, SEM, FT-IR, Antioxidant activity, Anticancer activity

1. Introduction

Nanoscience and nanotechnology are the most attractive area of research in materials science and engineering for the past two and half a decade. Nanomaterials have unique physical, chemical and catalytic properties. The performances of multifunctional nanomaterials are highly effective with their high surface to volume ratio. Metal oxide nanoparticles have good chemical and thermal stability and potential antimicrobial properties. Zinc oxide is an economical, inorganic, non-toxic material abundant in nature with wide range of cutting edge applications. It is a fascinating wide (3.37 eV), direct bandgap, n – type, refractive index of 2, the electron mobility of 50 – 60 cm²V⁻¹s⁻¹ and group II – IV metal oxide semiconductor with a high exciton binding energy of 60 meV[1–3].

The properties of zinc oxide nanoparticles rely on the defects of the materials such as oxygen vacancies. The addition impurity in zinc oxide nanoparticles with different doping concentrations is a smooth route to tune the properties of zinc oxide nanoparticles. Zinc oxide nanoparticles is normally doped elements such as Ag[3], Al[4–7], Cu[8,9] Ni[10], Co[11], Cd[12], Ce[13], Gd[14], Tb[15], Mn[16] and Mg[17]. The addition of magnesium (Mg²⁺) with ionic radius 0.72 Å is most suitable in zinc oxide lattice (Zn²⁺) with an ionic radius of 0.74 Å[18]. The

* Corresponding author: pricilla1510@gmail.com

<https://doi.org/10.15251/JOR.2022.185.637>

addition of magnesium enhances the optical and electrochemical properties of zinc oxide nanoparticles[19]. The multifunctional nature of magnesium doped zinc oxide nanoparticles with wide band gap have proved prospective material for a variety of applications such as photo catalysis, antimicrobial and anticancer applications[1,2,20–23]. The magnesium doped zinc oxide nanoparticles are prepared by different methods, such as co-precipitation method[22,24], auto combustion method[25,26] and green synthesis[17,27].

Motivated by the above facts, the present investigation intended to characterize the magnesium doped zinc oxide nanoparticles synthesized by the soft chemical method and to explore antioxidant potential and anticancer activity in breast cancer MDAMB231 cell line. The prepared nanoparticles were examined by X-ray diffraction, scanning electron microscopy, energy dispersive X-ray spectroscopy, UV–vis spectrometry, Fourier Transform Infrared Spectroscopy, and room temperature photo-luminescence measurements.

2. Materials and Methods

2.1. Chemicals

Zinc acetate dihydrate ($\text{Zn}(\text{CH}_3\text{COO})_2 \cdot 2\text{H}_2\text{O}$), Magnesium acetate tetrahydrate ($\text{Mg}(\text{CH}_3\text{COO})_2 \cdot 4\text{H}_2\text{O}$) and sodium hydroxide (NaOH) obtained from Merck Chemicals were used. Characterization was carried out in the recognized research laboratories.

Synthesis and characterization of magnesium doped zinc oxide nanoparticles

Magnesium doped zinc oxide nanoparticles with different concentrations (5 atomic % and 10 atomic %) were prepared by the soft chemical method. The obtained samples were annealed at 200°C for 2 h in a muffle furnace. The annealed samples were used for further analysis.

The experimental procedure was followed as per Srinivasan *et. al.*, [6]. The magnesium concentration 5 atomic % and 10 atomic % was added to zinc oxide for the samples were named as ‘MZ1’ and ‘MZ2’, respectively. The obtained samples ‘MZ1’ and ‘MZ2’ were annealed at 200°C for the samples were named as ‘MZ3’ and ‘MZ4’ respectively.

X-ray diffraction patterns of nanoparticles were recorded using Panalytical X pert PRO powder X-ray Diffractometer with Cu $K\alpha$ radiation ($\lambda = 1.54060 \text{ \AA}$) with a step size of 0.02° . The scanning electron microscope with EDAX (JEOL) was used to explore the surface morphology and to estimate the composition of the prepared nanoparticles.

UV-vis absorption spectra of the nanoparticles were recorded using JASCO, UV-vis spectrophotometer, USA. Fourier transform infrared spectrophotometer SHIMADZU (FT-IR 8400) was used to record FT-IR spectra of the samples. The room temperature photoluminescence (PL) spectra of the samples were recorded using a spectrofluorimeter.

The antioxidant potential and anticancer activity was explored with DPPH assay and MTT assay method. The procedure of the above methods was reported elsewhere[16].

3. Results and discussion

XRD patterns of magnesium doped zinc oxide nanoparticles prepared by a soft chemical method with different condition are shown in Figure 1. Analysis of XRD patterns exposed that the prepared samples were crystallized in hexagonal wurtzite phase with a space group P63mc. All the observed peaks in the patterns related to zinc oxide (100), (002), (101), (102), (110), (103), (112) and (201) planes and all the observed peaks were in agreement with the JCPDS data (card number: 36-1451).

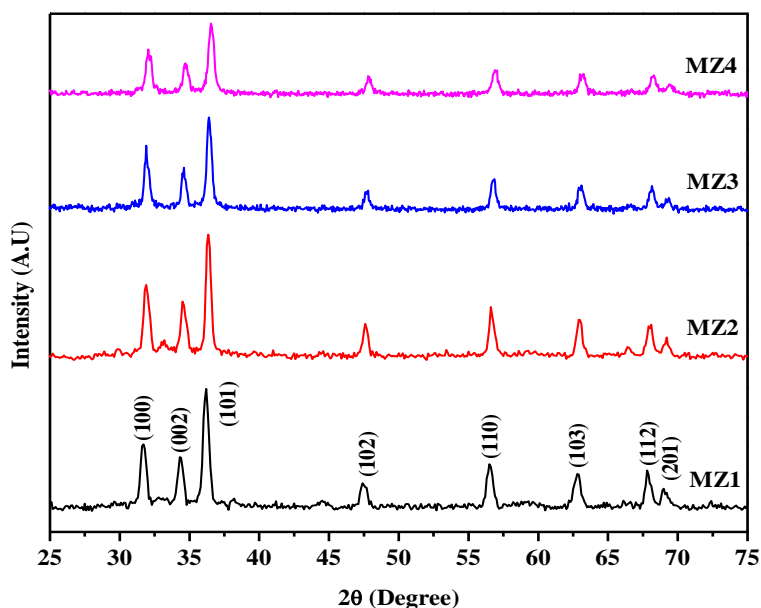


Fig. 1. XRD Patterns of magnesium doped zinc oxide nanoparticles: (MZ1) 5 atomic % Mg doped, (MZ2) 10 atomic % Mg doped, (MZ3) 5 atomic % Mg doped annealed at 200°C, (MZ4) 10 atomic % Mg doped annealed at 200°C.

All the XRD peaks were attributed to zinc oxide and no other impurity peaks were observed which indicates the better crystalline nature of the samples[1]. The absence of secondary peaks in the samples was suggested that magnesium was well incorporated with the host sites of zinc oxide.

The average grain size was estimated with Scherrer equation using the full width at the half maximum (FWHM) and angle of diffraction (θ)[28].

$$D = 0.9\lambda / (\beta \cos\theta) \quad (1)$$

where D - the average grain size of particles, β - full-width at half-maximum intensity and θ - angle of diffraction, respectively.

The lattice Parameters (a) and (c) of the prepared samples were calculated from following equations [29].

$$a = \lambda / (\sqrt{3} * \sin\theta)_{(100)} \quad (2)$$

$$c = \lambda / (\sin\theta)_{(002)} \quad (3)$$

The cell Volume of the samples was calculated from the formula[16].

$$V = 0.866 a^2c \quad (4)$$

where a, c are lattice constants.

The x-ray density of the samples was calculated from X-ray diffraction data using the following equation[16].

$$d_x = \frac{nM}{N_a * 2.598 * a^2 * c} \quad (5)$$

where n is the number of atoms per unit cell. M is the molecular weight of the synthesized nanoparticles (g/mol^{-1}) and a and c are lattice parameter (cm), N_a is Avogadro's number ($6.02 \times 10^{23} \text{ mol}^{-1}$).

The dislocation density of the prepared samples was calculated using the equation[29].

$$\delta = \frac{1}{D^2} \quad (6)$$

The microstrain in the lattice of the synthesized nanoparticles was estimated using the equation[16]

$$\varepsilon = \frac{\beta}{4 \tan \theta} \quad (7)$$

The atomic packing factor of synthesized nanoparticles were estimated the using equation[16].

$$APF = 2 \pi / (3\sqrt{3} * c) \quad (8)$$

The bond length of ZnO was estimated using the equation[16].

$$L = \sqrt{\left[\left(\frac{a^2}{3}\right) + \left(\frac{1}{2} - u\right)^2 * c^2\right]} \quad (9)$$

The estimated values from the XRD analysis are tabulated in Table 1. The calculated average grain size of samples MZ1, MZ2, MZ3 and MZ4 was 19.06 nm, 18.16 nm, 20.19 nm and 18.28 nm respectively.

The average grain size decreased with increase in magnesium concentration. The size reduction of sample MZ2 than sample MZ1 confirmed the addition of magnesium (Mg^{2+}) with an ionic radius 0.72 Å in zinc oxide lattice (Zn^{2+}) with an ionic radius of 0.74 Å [2]. The increased average grain size of samples MZ3 and MZ4 than MZ1 and MZ2 is due to the effect of annealing[30].

The annealing process reduced the surface energy of the samples MZ3 and MZ4 which increased the average grain size of the samples MZ3 and MZ4. The calculated lattice parameter and c/a ratio were consistent with the hexagonal wurtzite structure[29].

The calculated unit cell volume of sample MZ1, MZ2, MZ3 and MZ4 was 21.71 (Å)³, 21.31 (Å)³, 21.44 (Å)³ and 21.38 (Å)³ respectively. The cell volume decreased with increase in magnesium concentration. The decrease in the unit cell volume confirmed the presence of surface defects[2]. The calculated strain value of samples MZ1, MZ2, MZ3 and MZ4 was 0.0047, 0.0048, 0.0046 and 0.0044 respectively. The strain decreased with increase in magnesium concentration. The decrease in the value of strain reduced the average grain size of the sample MZ2 than sample MZ1. The effect of annealing reduced the value of strain in the samples MZ3 and MZ4 [30].

The estimated atomic packing factor values were 0.7571, 0.7576, 0.7543 and 0.7524 for the samples MZ1, MZ2, MZ3 and MZ4. The calculated atomic packing factors of the samples were in close agreement with zinc oxide nanoparticles[24]. The estimated bond length values were in good agreement with the reported values[2]. The geometrical parameters such as x-ray density, specific surface area and dislocation density were estimated and tabulated in Table 1.

Table 1. Analysis of XRD Patterns of Magnesium doped Zinc Oxide nanoparticles: (MZ1) 5 atomic % Mg doped, (MZ2) 10 atomic % Mg doped, (MZ3) 5 atomic % Mg doped annealed at 200°C, (MZ4) 10 atomic % Mg doped annealed at 200°C.

Sample	Crystal Size D (nm)	Lattice Parameter (Å°)		c/a ratio	Cell Volume V (Å ³)	X-ray density (dx) (gcm ⁻³)	Specific Surface Area	Dislocation density (δ) (10 ⁻⁴) nm ⁻²	Microstrain (ε)	APF	Bond Length (L) (Å°)
		a	c								
Undoped ZnO	43.0628	3.246	5.203	1.6027	19.8588	15.5475	0.0169	0.6599	0.0021	0.7544	1.9759
MZ1	18.1634	3.259	5.22	1.6016	21.7119	14.1702	0.0439	2.9328	0.0048	0.7571	1.9834
MZ2	19.0632	3.236	5.191	1.6042	21.3171	14.2996	0.0442	2.8379	0.0047	0.7516	1.9700
MZ3	18.2803	3.247	5.199	1.6008	21.4400	14.266	0.0456	3.0912	0.0049	0.7543	1.9758
MZ4	20.1994	3.239	5.19	1.6023	21.3875	14.261	0.0416	2.5118	0.0044	0.7524	1.9714

The variations of (101) diffraction peaks of the prepared samples are shown in Figure 2. The higher angle shift was observed. The higher angle shift was attributed to the presence of lattice strain in the prepared samples[31]. The shrinkage in the observed lattice parameters of the prepared samples confirmed the presence of lattice strain.

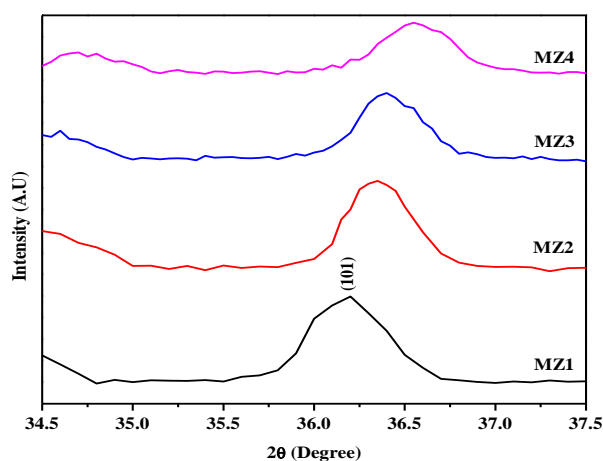


Fig. 2. Variation of (101) diffraction peak of magnesium doped zinc oxide nanoparticles: (MZ1) 5 atomic % Mg doped, (MZ2) 10 atomic % Mg doped, (MZ3) 5 atomic % Mg doped annealed at 200°C, (MZ4) 10 atomic % Mg doped annealed at 200°C.

SEM micrographs of magnesium doped zinc oxide nanoparticles prepared by a soft chemical method with different condition are shown in Figure 3. The formation of rod shape (sample MZ1, MZ2 and MZ4), flower shape (sample MZ3) was observed from the SEM micrographs. The SEM micrographs exposed the agglomeration of prepared samples.

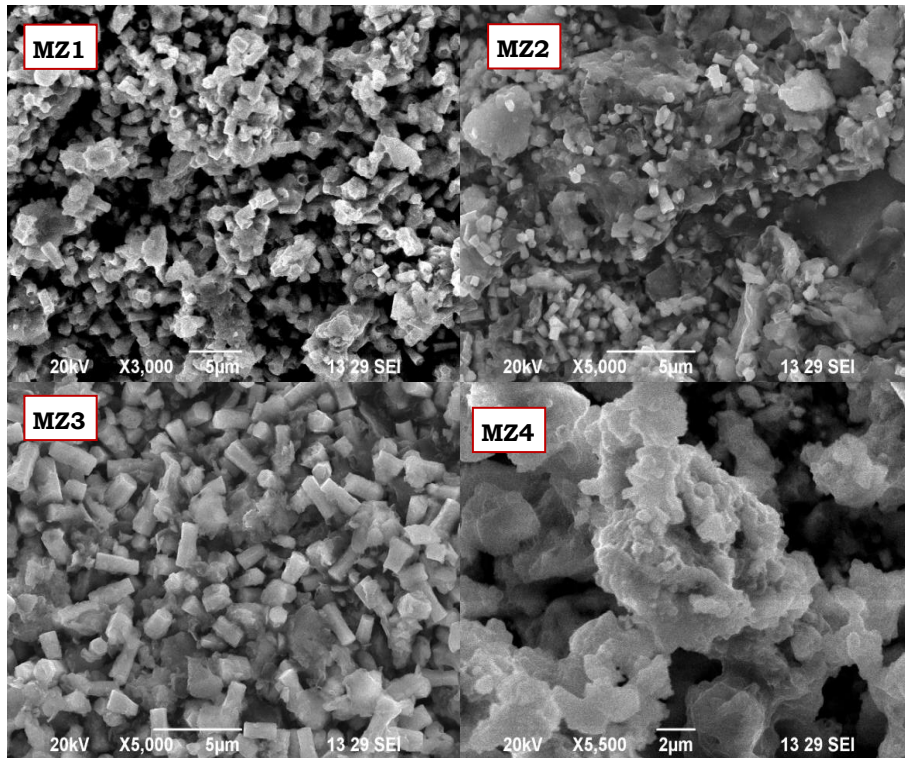


Fig. 3. SEM Analysis of magnesium doped zinc oxide nanoparticles: (MZ1) 5 atomic % Mg doped, (MZ2) 10 atomic % Mg doped, (MZ3) 5 atomic % Mg doped annealed at 200°C, (MZ4) 10 atomic % Mg doped annealed at 200°C.

The agglomeration initiated due to the presence of high surface energy in the prepared samples[24]. The addition of magnesium inhibited the growth of prepared nanoparticles, which was confirmed with size reduction from XRD analysis. The effect of annealing reduced the surface energy and altered the morphology of the prepared samples of magnesium doped zinc oxide nanoparticles.

EDAX spectrum of 10 atomic % magnesium doped zinc oxide nanoparticles (MZ2) prepared by the soft chemical method is shown in Figure 4. The EDAX spectrum revealed that the prepared sample has a stoichiometric ratio of constituent elements, zinc, magnesium and oxygen. No other elements present in the prepared sample confirmed the phase purity of the prepared magnesium doped zinc oxide nanoparticles[21].

Element	Weight %	Atomic %	Weight % Sigma
O K	37.72	70.93	0.96
Mg K	0.52	0.64	0.44
Zn K	61.76	28.43	0.99

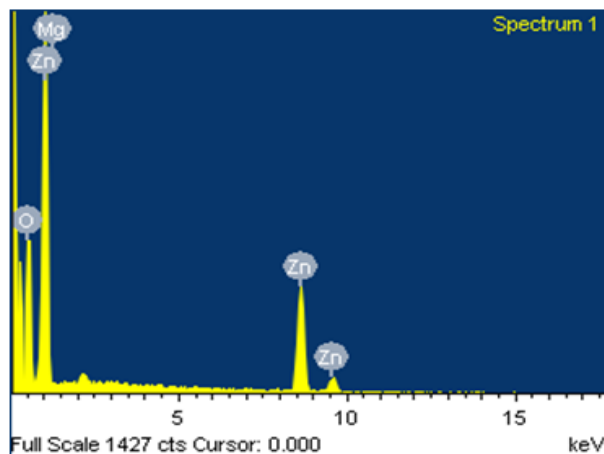


Fig. 4. EDAX spectrum of (MZ2) 10 atomic % Mg doped zinc oxide nanoparticles.

UV-vis spectrum of sample MZ1 and sample MZ2 are as shown in Figure 5. The absorption wavelengths were observed at 363 nm and 366 nm for the sample MZ1 and sample MZ3 respectively. A red shift was observed in the absorption edges of the samples and the band gap energy was decreased[32].

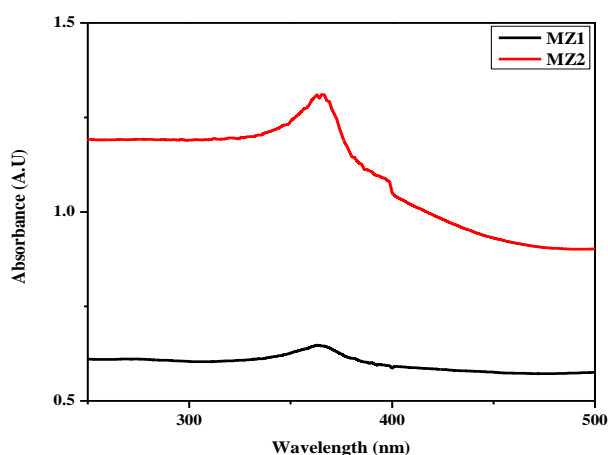


Fig. 5. UV-vis spectra of magnesium doped zinc oxide nanoparticles: (MZ1) 5 atomic % Mg doped and (MZ2) 10 atomic % Mg doped.

The band gap energy was estimated using equation[16]

$$E = 1240/\lambda \text{ (absorption)} \quad (10)$$

The calculated band gap energy of sample MZ1 and sample MZ3 were 3.41 e V and 3.38 e V. The reduction in the band gap values was attributed with strong quantum confinement and enhanced the surface to volume ratio. The red shift and decrease in the band gap values were confirmed the addition of magnesium in zinc oxide lattice[24].

FT-IR spectra of magnesium doped zinc oxide nanoparticles prepared by a soft chemical method with different condition are shown in Figure 6. The FTIR spectra were recorded in between 400 cm^{-1} – 4000 cm^{-1} using the KBr method at room temperature. The functional group analysis of the FTIR spectra confirmed the presence of various chemical functional groups.

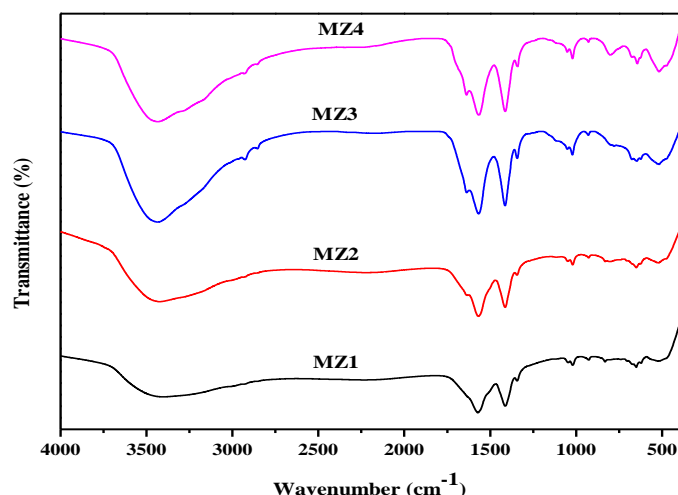


Fig. 6. FTIR Spectra of magnesium doped zinc oxide nanoparticles: (MZ1) 5 atomic % Mg doped, (MZ2) 10 atomic % Mg doped, (MZ3) 5 atomic % Mg doped annealed at 200°C, (MZ4) 10 atomic % Mg doped annealed at 200°C.

The observed peaks were at 3400 cm^{-1} , 1586 cm^{-1} , 1427 cm^{-1} , 1341 cm^{-1} , 1025 cm^{-1} , 927 cm^{-1} , 832 cm^{-1} , 653 cm^{-1} and 496 cm^{-1} . The peaks at 3400 cm^{-1} and 1586 cm^{-1} were assigned for O-H stretching and O-H bending respectively. The peaks at 1427 cm^{-1} , 1341 cm^{-1} and 1025 cm^{-1} were attributed to C=O bonds.

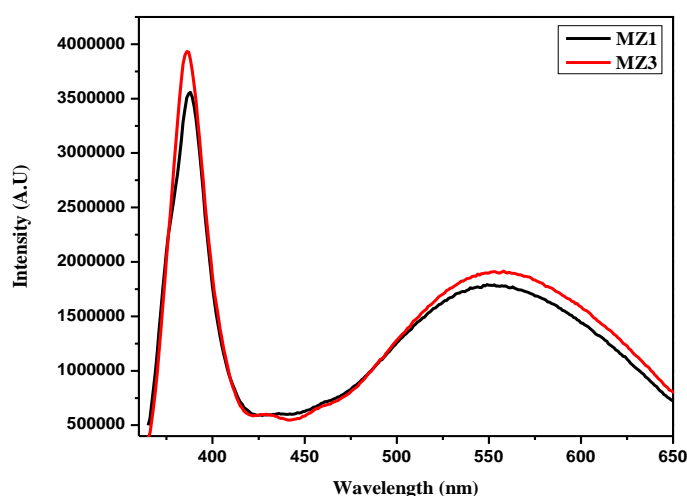


Fig. 7. Room temperature PL spectra of magnesium doped zinc oxide nanoparticles: (MZ1) 5 atomic % Mg doped, (MZ3) 5 atomic % Mg doped annealed at 200°C.

The peaks observed at 927 cm^{-1} , 832 cm^{-1} and 653 cm^{-1} were assigned for Mg-O bonds [18]. The peak observed at 469 cm^{-1} was confirmed the presence of Zn-O bond [33]. The analysis of the FTIR spectra were established the presence of functional groups for Zn-O bond and Mg-O bonds respectively.

The room temperature photoluminescence spectra of magnesium (5 atomic %) doped zinc oxide nanoparticles (sample MZ1) and magnesium (5 atomic %) doped zinc oxide annealed with 200 °C (sample MZ3) are shown in Figure 7. The PL spectroscopy is an effective tool for the defect analysis of metal oxide nanomaterials.

Two emission bands were observed in both sample MZ1 and sample MZ3. The emission peaks were observed at 387 nm in the ultraviolet region and 557 nm in the visible region. The

strong ultraviolet emission peak at 387 nm originated from the near band edge emission (NBE). This near band edge emission was endorsed to free exciton emission[34].

A green emission peak at 557 nm was a defect emission band. The green emission peak was related to the defect of oxygen vacancies[1,23]. There was an increase in the intensity of sample MZ3 than sample MZ1. The increase in the intensity of sample MZ3 was due to the reduction in the grain boundaries[30].

DPPH assay method was employed to test the antioxidant potential of the prepared samples MZ1 and MZ2 with standard ascorbic acid. The antioxidant potential graph is as shown in Figure 8. The different concentration of nanoparticles such as 5, 10, 15, 20, 25 and 30 $\mu\text{g/ml}$ was used for the analysis. A linear relationship between concentrations and antioxidant activity was observed. The sample MZ2 exposed better antioxidant potential with higher concentration (30 $\mu\text{g/ml}$).

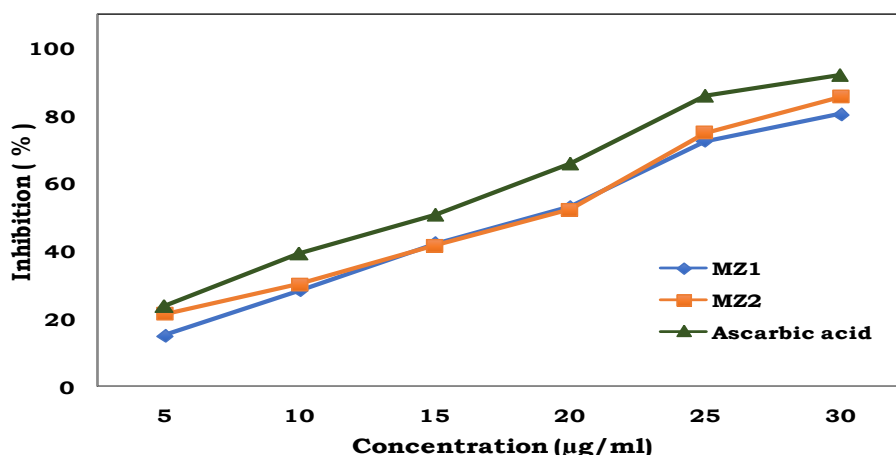


Fig. 8. DPPH radical scavenging activity of undoped and Mg (5 atomic % & 10 atomic %) doped zinc oxide nanoparticles.

MTT assay method was used to examine the anticancer activity of the prepared samples MZ1, MZ2 and Doxorubicin drug against the breast cancer MDAMB231 cancer cell line. The cell viability percentage graph is as shown in Figure 9. The different concentration of nanoparticles such as 5, 10, 15, 20, 25 and 30 $\mu\text{g/ml}$ was used for the analysis. The cell viability percentage was estimated[22]. There was a reciprocal relationship observed between cell viability percentage and concentration of nanoparticles. The sample MZ2 with concentration 30 $\mu\text{g/ml}$ was more effective than standard drug Doxorubicin.

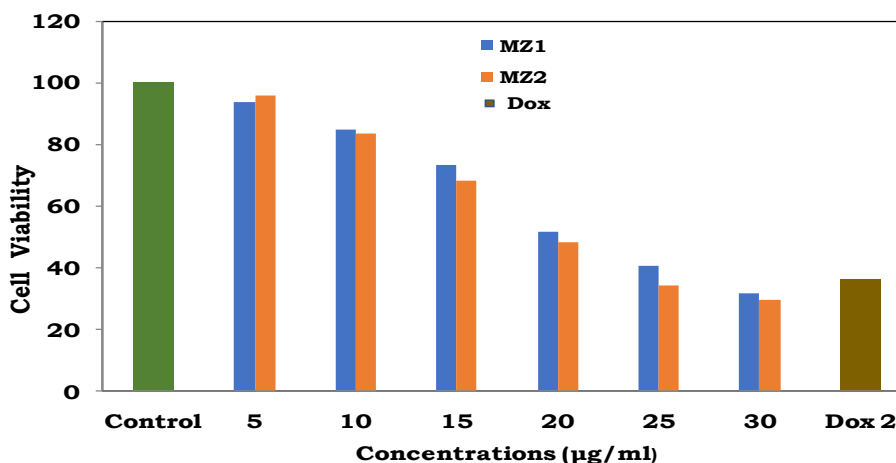


Fig. 9. Cancer activity of undoped and Mg (5 atomic % & 10 atomic %) doped zinc oxide nanoparticles.

4. Conclusion

Magnesium doped zinc oxide nanoparticles were successfully prepared by a soft chemical method. The prepared nanoparticles were annealed at 200 °C for 2 h. The XRD analysis confirmed the formation of hexagonal wurtzite phase with a space group P63mc for all samples and no impurity phase was observed. The calculated average grain size of samples MZ1, MZ2, MZ3 and MZ4 was 19.06 nm, 18.16 nm, 20.19 nm and 18.28 nm respectively.

The SEM micrographs analysis exposed the surface agglomeration of prepared samples. The annealing of prepared samples reduced the surface energy and altered the surface morphology. EDAX spectrum revealed the phase purity of the prepared samples.

A red shift was observed in the absorption edges of the samples and the band gap energy was decreased with strong quantum confinement from the UV-vis analysis. The estimated band gap energy of sample MZ1 and sample MZ3 were 3.41 e V and 3.38 e V.

The analysis of the FTIR spectra established the presence of functional groups for Zn-O bond at 469 cm⁻¹ and Mg-O bonds at 832 cm⁻¹ respectively. The PL analysis exhibited a strong UV emission peak at 387 nm and a defect related green emission peak at 557 nm.

The sample MZ2 with concentration 30 µg/ml displayed excellent antioxidant potential and anticancer activity. The results provide a ray of light that the next generation cancer drugs could be developed based on metal oxide nanoparticles.

References

- [1] K. V. Karthik, A. V. Raghu, K.R. Reddy, R. Ravishankar, M. Sangeeta, N.P. Shetti, C.V. Reddy, *Chemosphere*. 287 (2022) 132081; <https://doi.org/10.1016/j.chemosphere.2021.132081>
- [2] I.S. Okeke, K.K. Agwu, A.A. Ubachukwu, I.G. Madiba, M. Maaza, G.M. Whyte, *Vacuum*. 187 (2021) 110110; <https://doi.org/10.1016/j.vacuum.2021.110110>
- [3] M.A. Kareem, I.T. Bello, H.A. Shittu, P. Sivaprakash, O. Adedokun, S. Arumugam, *Clean. Mater.* 3 (2022) 100041; <https://doi.org/10.1016/j.clema.2022.100041>
- [4] K.S. Khashan, G.M. Sulaiman, S.A. Hussain, T.R. Marzoog, M.S. Jabir, J. Inorg. Organomet. Polym. Mater. 30 (2020) 3677-3693; <https://doi.org/10.1007/s10904-020-01522-9>
- [5] R. Mahdavi, S.S.A. Talesh, *Adv. Powder Technol.* 28 (2017) 1418-1425; <https://doi.org/10.1016/j.appt.2017.03.014>
- [6] J.C.Kaannan. N. Srinivasan, *Mater. Sci.* (2015); <https://doi.org/10.1515/msp-2015-0021>
- [7] N. Srinivasan, J. C. Kannan. S. Satheeskumar, *Int. J. PharmTech Res.* 7 (2015) 287 - 290
- [8] N. Srinivasan, *J. Surf. Investig.* 13 (2019); <https://doi.org/10.1134/S1027451019060508>
- [9] N. Srinivasan, M. Revathi, P. Pachamuthu, *Optik (Stuttg.)*. 130 (2017) 422-426; <https://doi.org/10.1016/j.ijleo.2016.10.080>
- [10] K. Xu, C. Liu, R. Chen, X. Fang, X. Wu, J. Liu, *Phys. B Condens. Matter.* 502 (2016) 155-159; <https://doi.org/10.1016/j.physb.2016.07.017>
- [11] M. Goswami, *Opt. Mater. (Amst.)*. 109 (2020) 110400; <https://doi.org/10.1016/j.optmat.2020.110400>
- [12] T.S. Perundevi, A. Karthika, S. Ramalakshmi, *Mater. Today Proc.* 51 (2022) 1738-1742; <https://doi.org/10.1016/j.matpr.2020.11.721>
- [13] J. Lang, J. Wang, Q. Zhang, X. Li, Q. Han, M. Wei, Y. Sui, D. Wang, J. Yang, *Ceram. Int.* 42 (2016) 14175-14181; <https://doi.org/10.1016/j.ceramint.2016.06.042>
- [14] M. Mazhdi, M.J. Tafreshi, *Nucl. Instruments Methods Phys. Res. Sect. A Accel. Spectrometers, Detect. Assoc. Equip.* 959 (2020) 163604; <https://doi.org/10.1016/j.nima.2020.163604>
- [15] P. Kumar, V. Chauhan, A.G. Joshi, P.C. Pandey, *Optik (Stuttg.)*. 216 (2020) 164839; <https://doi.org/10.1016/j.ijleo.2020.164839>
- [16] P. Pachamuthu, A. Pricilla Jeyakumari, N. Srinivasan, R. Chandrasekaran, K. Revathi, P.

- Karuppannan, J. Indian Chem. Soc. 99 (2022) 100342; <https://doi.org/10.1016/j.jics.2022.100342>
- [17] J.N. D'Souza, G.K. Nagaraja, K. Meghana Navada, S. Kouser, D.J. Manasa, Ceram. Int. 47 (2021) 29620-29630; <https://doi.org/10.1016/j.ceramint.2021.07.131>
- [18] P. Rajput, P. Singh, P. Vashishtha, Kamni, Bull. Mater. Sci. 44 (2021); <https://doi.org/10.1007/s12034-021-02438-x>
- [19] M. Carofiglio, S. Barui, V. Cauda, M. Laurenti, Appl. Sci. 10 (2020); <https://doi.org/10.3390/app10155194>
- [20] G. Kasi, K. Viswanathan, K. Sadeghi, J. Seo, Prog. Org. Coatings. 133 (2019) 309-315; <https://doi.org/10.1016/j.porgcoat.2019.04.066>
- [21] R. Subbiah, S. Muthukumar, V. Raja, Bionanoscience. 11 (2021) 1127-1141; <https://doi.org/10.1007/s12668-021-00890-x>
- [22] K. Chandrasekaran, K. Varaprasad, S.K. Venugopal, L. Arun, A.S.H. Hameed, Bionanoscience. 10 (2020) 106-111; <https://doi.org/10.1007/s12668-019-00696-y>
- [23] J. Gupta, D. Bahadur, ACS Omega. 3 (2018) 2956-2965; <https://doi.org/10.1021/acsomega.7b01953>
- [24] K. Pradeev raj, K. Sadaiyandi, A. Kennedy, S. Sagadevan, Z.Z. Chowdhury, M.R. Bin Johan, F.A. Aziz, R.F. Rafique, R. Thamiz Selvi, R. Rathina bala, Nanoscale Res. Lett. 13 (2018); <https://doi.org/10.1186/s11671-018-2643-x>
- [25] N. Pushpa, M.K. Kokila, K.R. Nagabhushana, Nucl. Instruments Methods Phys. Res. Sect. B Beam Interact. with Mater. Atoms. 379 (2016) 62-68; <https://doi.org/10.1016/j.nimb.2016.04.042>
- [26] Kalyani, V. Jaiswal, R.B. Rastogi, D. Kumar, Appl. Nanosci. 7 (2017) 275-281; <https://doi.org/10.1007/s13204-015-0471-1>
- [27] L. Umaralikhan, M.J.M. Jaffar, J. Mater. Sci. Mater. Electron. 28 (2017) 7677-7685; <https://doi.org/10.1007/s10854-017-6461-1>
- [28] S.N.K.J.S.S. S, Indian Chem. Soc. (2016).
- [29] M.A. Vargas, E.M. Rivera-Muñoz, J.E. Diosa, E.E. Mosquera, J.E. Rodríguez-Páez, Ceram. Int. 47 (2021) 15668-15681; <https://doi.org/10.1016/j.ceramint.2021.02.137>
- [30] A.N. Mallika, A.R. Reddy, K.V. Reddy, J. Adv. Ceram. 4 (2015) 123-129; <https://doi.org/10.1007/s40145-015-0142-4>
- [31] R. Sagheer, M. Khalil, V. Abbas, Z.N. Kayani, U. Tariq, F. Ashraf, Optik (Stuttg). 200 (2020); <https://doi.org/10.1016/j.ijleo.2019.163428>
- [32] S. V. Elangovan, N. Sivakumar, V. Chandramohan, J. Mater. Sci. Mater. Electron. 26 (2015) 8753-8759; <https://doi.org/10.1007/s10854-015-3553-7>
- [33] F. Adam, A. Himawan, M. Aswad, D. Tahir, J. Phys. Conf. Ser. 1317 (2019); <https://doi.org/10.1088/1742-6596/1317/1/012051>
- [34] V. V. Kutwade, K.P. Gattu, A.S. Dive, M.E. Sonawane, D.A. Tonpe, R. Sharma, J. Mater. Sci. Mater. Electron. 32 (2021) 6475-6486; <https://doi.org/10.1007/s10854-021-05364-0>